Theoretical Study of the Dissociation of Nitric Acid at a Model Aqueous Surface

Roberto Bianco,*,† Shuzhi Wang,† and James T. Hynes*,†,‡

Department of Chemistry and Biochemistry, University of Colorado, Boulder, Colorado 80309-0215, and Département de Chimie, CNRS UMR 8640 PASTEUR, Ecole Normale Supérieure, 24 rue Lhomond, Paris 75231, France

Received: June 28, 2007; In Final Form: August 2, 2007

The issue of acid dissociation of nitric acid at an aqueous surface is relevant in various portions of the atmosphere in connection with ozone depletion. This proton-transfer reaction is studied here via electronic structure calculations at the HF/SBK+(d) level of theory on the $HNO_3 \cdot (H_2O)_3$ model reaction system embedded in clusters comprising 33, 40, 45, and 50 classical, polarizable waters with an increasing degree of solvation of the nitrate group. Free energy estimates for all the cases examined favor undissociated, molecular nitric acid over the 0−300 K temperature range, including that relevant for the upper troposphere, where it is connected to the issue of the mechanism of nitric acid uptake by water ice aerosols. The presence of molecular HNO_3 at 300 K at the surface is further supported by vibrational band assignments in good agreement with a very recent surface-sensitive vibrational spectroscopy study of diluted HNO_3/H_2O solutions.

1. Introduction

Nitric acid HNO_3 is an important chemical actor in a wide span of heterogeneous reactions important in various atmospheric contexts. In the stratosphere, nitrate aerosols (NAT, nitric acid trihydrate) form one of the sites for heterogeneous chlorine chemistry related to ozone depletion.[1] Further, nitric acid is itself a product of these chlorine reactions, e.g., that of chlorine nitrate with hydrochloric acid.[1,2] The troposphere provides numerous instances of heterogeneous nitric acid chemistry. For example, the reaction of NO with (molecular) nitric acid on aqueous surfaces has been shown to generate reactive nitrogen species ("renoxification") significant in tropospheric pollution,[3] whereas in the marine troposphere, uptake of nitric acid by sea-salt aerosols is believed to be an important NO_x removal process.[4]

Another tropospheric role for HNO_3, of special interest in the present work, involves its uptake by water-ice aerosol particles in the upper troposphere (UT), where cirrus clouds are formed, as are airplane condensation trails (contrails).[5−14] This uptake is important for ozone concentrations for several reasons. First, HNO_3 can generate NO_2, which ultimately produces ozone; the uptake of HNO_3 by water-ice particles removes ("sequesters") HNO_3 from this activity, ultimately affecting ozone production levels.[6] Second, heterogeneous reactions occurring on the surface of the UT particles such as the hydrolysis of chlorine nitrate, $ClONO_2$, and the reaction of $ClONO_2$ with hydrochloric acid, HCl, related to ozone depletion, can occur on ice particles but are much less efficient on HNO_3-coated ice. Such chlorine activation reactions occurring on cirrus clouds in the tropopause region may have an important impact on ozone.[7−9]

In the present work, we examine theoretically the possibility of acid dissociation of nitric acid at an aqueous surface (eq 1), a proton-transfer reaction of the acid with a water molecule to produce the hydronium ion H_3O^+ and the nitrate ion NO_3^-

$$HNO_3 + H_2O \rightarrow NO_3^- + H_3O^+ \qquad (1)$$

This acid ionization has been suggested by Abbatt[10] as a chemisorptive mechanism involved in the significant HNO_3 uptake in the UT.[10−14] It has also been invoked in the sea-salt aerosol uptake of HNO_3[4] and is important for the renoxification process, which involves molecular HNO_3 rather than the acid ionization product NO_3^-.[3]

It should be noted that because HNO_3 is a much weaker acid (in bulk solution) than is sulfuric acid (H_2SO_4),[15] which was predicted to acid ionize at an aqueous surface only under certain lower temperature conditions,[16] it cannot be taken for granted *a priori* that HNO_3 will acid ionize in the surface layer. Although laboratory experiments[17−22] suggest that molecular nitric acid is dominant at the surfaces of highly concentrated nitric acid solutions (for which molecular nitric acid is also dominant in the bulk[23,24]), the situation at lower concentrations—relevant for the conditions of the present study—has been less clear. Several surface-sensitive sum frequency generation studies from the Schultz[18,19,21] and Richmond[22] groups bear upon this issue and are discussed within in connection with our results.

At low coverage of HNO_3 on UT ice aerosols—up to about 0.1 monolayer[10,12]—only a single HNO_3 molecule need be considered, which is the case studied here via electronic structure methods similar to those employed previously[25] for the acids HCl,[26] HBr,[26] and especially H_2SO_4.[16,27] We focus on several different degrees of solvation of the HNO_3 at an aqueous surface. The feasibility of the acid ionization equation (1) is assessed by reaction free energy calculations, over a wide temperature range 0−300 K. This range includes that relevant for the UT 206−264 K (5−15 km),[28] and at its upper end makes contact with recent spectroscopic experiments.[22]

The outline of the remainder of this paper is as follows. The methodology is presented in section 2, with the results discussed in section 3. Certain key vibrational bands connecting our results with recent experiments are discussed in section 4, and concluding remarks are offered in section 5.

* Corresponding authors. E-mail: R.B., roberto.bianco@colorado.edu; J.T.H., hynes@spot.colorado.edu, hynes@chimie.ens.fr.

† University of Colorado.

‡ Ecole Normale Supérieure.

10.1021/jp075054a CCC: $37.00
Published on Web 10/05/2007

TABLE 1: HNO_3 Structure[a]

	exp[b]	HF[c]	CCSD[d]
N═O_4	1.211	1.204	1.216
N═O_3	1.199	1.187	1.200
N−OH	1.406	1.345	1.418
O−H	0.964	0.964	0.969
∠HON	102.2	104.8	101.5
∠O−N═O_4	115.4	116.2	115.9
∠O−N═O_3	114.0	114.9	113.9

[a] HNO_3 is planar. See Figure 1 for atomic labeling. Bond lengths in Å, angles in deg. [b] Experimental values.[63] [c] This work, HF/SBK+(d). [d] Reference 64.

2. Methodology

Here we only highlight the key features of our methodology and refer the reader to ref 16 on the analogous H_2SO_4 problem for details. The HNO_3•$(H_2O)_3$•W_n model reaction system (MRS) comprises a HNO_3•$(H_2O)_3$ core reaction system (CRS), which is treated quantum-chemically at the HF/SBK+(d) (henceforth HF) level of theory, and which is embedded in a W_n cluster of classical, polarizable waters of fixed internal structure (effective fragment potentials, EFP).[29] Upon formation of the NO_3^-•H_3O^+•$(H_2O)_2$ contact ion pair (CIP), the hydronium ion is screened by the other two quantum waters from the classical waters in the lattice, thus preventing the shortening of one of the two W···HOH_2^+ hydrogen (H)-bonds to an unreasonable 0.5 Å, a pathology typical of this particular interaction.[16] The SBK[30] effective core potential basis set is complemented by polarization ("d")[31] (exponent 0.8 for both N and O) and diffusion ("+")[32] (N 0.0639 and O 0.0845 exponents) functions. The quantum chemistry package GAMESS[33] was used for the calculations. The HF optimized structure of HNO_3 is reported in Table 1.

In the CRS, only the proton-accepting water is solvated by two other quantum waters, whereas the nitrate oxygens are H-bonded to EFP waters. An analogous situation has been examined for the MD simulation of the dissociation of HNO_3 in a small water cluster with mixed quantum and TIP4P waters,[34] where the replacement of two TIP4P waters H-bonded to NO_2 by quantum waters had negligible effect on the dissociation kinetics of HNO_3. For the cases examined here, the effect would presumably be further reduced, because EFP waters are polarizable, whereas TIP4P waters are not. We have verified that the current HF level of theory H-bonding by the W-EFPs to the nitro group of HNO_3 or NO_3^- is structurally very similar to that by quantum waters for the cyclic HNO_3•$(H_2O)_2$ and NO_3^-•H_2O water clusters (see Supporting Information).

As described in detail in section 3, four different size clusters are used, corresponding to different degrees of nitrate group solvation in the surface region. The cluster for the case with maximum solvation of the nitrate group, namely HNO_3•$(H_2O)_3$•W_{50}, was assembled by first embedding the CRS into a hexagonal lattice of oxygen atoms and then assigning the positions of the hydrogens starting with the first solvation shell and moving outward.[16] The other three cases examined, with decreasing solvation of the nitrate group, have been derived by removing waters from the most solvated case. In each case, the transition state region of the potential energy surface for the acid dissociation path was located by constrained optimization via stepwise reduction of the H_2O···H−ONO_2 H-bond toward formation of ^+H_2O−H···ONO_2^-. After full optimization of the transition state (TS), the corresponding reactant complex (RC) and product complex (PC) were identified via an intrinsic reaction coordinate path[35] calculation and further energy minimization. All TS, RC, and PC were characterized by a Hessian calculation. Structures and vibrational modes were visualized with Molden.[36]

TABLE 2: HNO_3 Vibrational Frequencies[a]

	gas[b]	HF[c]	s.f.[d]	mode[e]
ν_1	3550	4012.46	0.8847	HO str
ν_2	1708	1930.28	0.8848	NO_2 as-str
ν_3	1331	1586.24	0.8391	NO_2 s-str
ν_4	1325	1485.11	0.8922	H−O−N bnd
ν_5	879	1128.56	0.7789	(H)O−N str
ν_6	647	761.46	0.8497	NO_2 sciss
ν_7	579	667.30	0.8677	(H)O−N−O bnd
ν_8	762	867.46	0.8784	NO_2 wag
ν_9	456	525.19	0.8683	HONO tor

[a] Frequencies in cm^{-1}. C_s point group symmetry. Modes ν_1−ν_7 are of type A′, whereas modes ν_8 and ν_9 are of type A″. [b] Gas phase. Modes 1−8: Shimanouchi, T. *Tables of Molecular Vibrational Frequencies*, Consolidated Volume 1, NSRDS NBS-39. Mode 9: Huber, K.P.; Herzberg, G. *Molecular Spectra and Molecular Structure. IV. Constants of Diatomic Molecules*; Van Nostrand Reinhold Co.: New York, 1979. [c] This work. Unscaled HF/SBK+(d) frequencies. [d] Mode-specific scaling factor (s.f.). Average scaling factor: 0.8604. [e] Mode description: str = stretching, s = symmetric, as = asymmetric, bnd = bending, sciss = scissoring, wag = wagging, tor = torsion, def = deformation.

TABLE 3: H_2O Vibrational Frequencies[a]

	gas[b]	HF[c]	s.f.[d]	mode[e]
ν_1	3657	4046.64	0.9037	O−H s-str
ν_2	1595	1756.19	0.9082	H−O−H bnd
ν_3	3756	4160.76	0.9027	O−H as-str

[a] Frequencies in cm^{-1}. C_{2v} point group symmetry. Modes ν_1 and ν_2 are of type A_1, whereas mode ν_3 is of type B_1. [b] Experimental, gas phase.[65] [c] This work. Unscaled HF/SBK+(d) frequencies. [d] Mode-specific scaling factor (s.f.). [e] Mode description (see Table 2.)

The reaction free energies associated with the production of the NO_3^-•H_3O^+ CIP were calculated as

$$\Delta G = (E_{PC} - E_{RC}) + (ZPE_{PC} - ZPE_{RC}) + (H_{PC}^{therm} - H_{RC}^{therm}) - T(S_{PC} - S_{RC}) \quad (2)$$

where E is the energy at 0 K, ZPE is the zero point energy, H^{therm} is the thermal contribution from translational, rotational, and vibrational motions, and S is the entropy contribution from these motions. The ZPEs and the vibrational contributions to the thermodynamic quantities from intermolecular modes were calculated using frequencies scaled by the average factors 1.0962 and 0.9173, respectively, for frequencies below and above 1000 cm^{-1}, obtained via comparison between MP2/aug-cc-pVDZ[37] and HF frequencies for the cyclic water tetramer as detailed in ref 16. The intramolecular modes of HNO_3, H_2O, NO_3^-, and H_3O^+ in the CRS of each RC and PC have been identified via an automated analysis of the atomic motion components and confirmed visually via Molden,[36] and each mode has been scaled according to its mode-specific scaling factor as indicated in Tables 2−5.

As in ref 16 for the H_2SO_4 first acid ionization, electron correlation effects for the 0 K reaction energies for the nitric acid proton-transfer (eq 1) were estimated in two steps. The first step compares the electronic contributions (PA_e) to the gas-phase proton affinities (PA) of H_2O and NO_3^- at the HF, MP2/SBK+(d) (henceforth MP2), and CBS[38] levels, as shown in Table 6. The MP2 value for the difference $PA_e(NO_3^-) - PA_e(H_2O)$, which is the reaction energy ΔE(0 K) for the $HNO_3 + H_2O \rightarrow NO_3^- + H_3O^+$ gas-phase reaction, is 4.92 kcal/mol less than the CBS value 159.60 kcal/mol. This indicates a 4.92

TABLE 4: NO_3^- Vibrational Frequencies[a]

	gas[b]	HF[c]	s.f.[d]	mode[e]
ν_1	1043	1218.43	0.8560	N═O s-str
ν_2	830	937.64	0.8852	out-of-plane def
ν_3	1370	1579.50	0.8674	N═O as-str
ν_4	723	769.12	0.9400	in-plane bnd

[a] Frequencies in cm^{-1}. D_{3h} point group symmetry. Mode ν_1 is of type A'_1, mode ν_2 is of type A''_2, and modes ν_3 and ν_4 are of type E′. [b] Experimental, gas phase.[66] [c] This work. Unscaled HF/SBK+(d) frequencies. [d] Mode-specific scaling factor (s.f.). [e] Mode description (see Table 2.)

TABLE 5: H_3O^+ Vibrational Frequencies[a]

	gas[b]	HF[c]	s.f.[d]	mode[e]
ν_1	3491.17	3753.58	0.9301	O−H s-str
ν_2	954.40	992.04	0.9621	def
ν_3	3574.29	3855.60	0.9270	O−H as-str
ν_4	1693.87	1783.24	0.9499	def

[a] Frequencies in cm^{-1}. C_{3v} point group symmetry. Modes ν_1 and ν_2 are of type A_1, whereas modes ν_3 and ν_4 are of type E. [b] Experimental, gas phase.[67] Table 4 therein, (−) series. [c] This work. Unscaled HF/SBK+(d) frequencies. [d] Mode-specific scaling factor (s.f.). [e] Mode description (see Table 2.)

TABLE 6: Proton Affinities of H_2O and NO_3^- (Electronic Contributions)[a]

	CBS[b]	HF[c]	MP2[d]
PA_e (H_2O)	171.56	169.11	165.87
PA_e (NO_3^-)	331.16	322.74	320.55
ΔPA_e	159.60	153.63	154.68

[a] Energies in kcal/mol. [b] Reference 68. [c] This work: HF/SBK+(d) and MP2/SBK+(d).

TABLE 7: Electron Correlation Effects for $HNO_3\cdot(H_2O)_n \rightarrow NO_3^-\cdot H_3O^+\cdot(H_2O)_{n-1}$[a]

	n	ΔE_{HF}	ΔE_{MP2}	Δ[b]	corr[c]
I	11	6.21	0.59	−5.62	−0.70
II	14	1.68	−5.21	−6.89	−1.97
III	14	3.42	−2.54	−5.96	−1.04
IV	13	0.42	−5.55	−5.97	−1.05

[a] Energies in kcal/mol. [b] $\Delta = \Delta E_{MP2} - \Delta E_{HF}$. [c] corr $= \Delta + 4.92$ (see end of section 2).

kcal/mol bias in the MP2 calculations *in favor* of the proton transfer from HNO_3 to H_2O compared to the CBS result. Thus, to correct the "intrinsic" deficiencies of the MP2 estimates of electron correlation effects in the aqueous surface calculations, we must apply the correction +4.92 kcal/mol to the 0 K reaction energy. The second step assesses electron correlation effects for stable reactant and product complexes found in the HF calculations for the several aqueous surface cases (cf. Table 7). These calculations, which are performed on a significant portion of the MRS for the various cases (see Figures 2−5 and Supporting Information), indicate non-negligible electron correlation effects on the 0 K HF reaction energies. These effects are negative contributions, in the range of 5−7 kcal/mol in magnitude, favoring the acid dissociation of HNO_3 even more than the HF values. However, the considerations of the first portion of this paragraph indicate that these need to be corrected by +4.92 kcal/mol. The *net* effect is that the 0 K HF reaction energies for the HNO_3 acid dissociation are corrected by −1.97 to −0.70 kcal/mol in the various cases, corrections that are similar in magnitude to those applied in ref 16 for H_2SO_4. We also note that the small corrections due to electron correlation are consistent with those found in ref 2, where we have shown that for the $HCl\cdot ClONO_2\cdot(H_2O)_9$ model reaction system, treated fully quantum-chemically, without extra classical waters, the MP2//HF energy at 0 K along the whole HF reaction path (calculated with the same basis set) is only ∼1 kcal/mol higher than the HF energy (see Figure 2 in ref 2), thus supporting our current methodology.

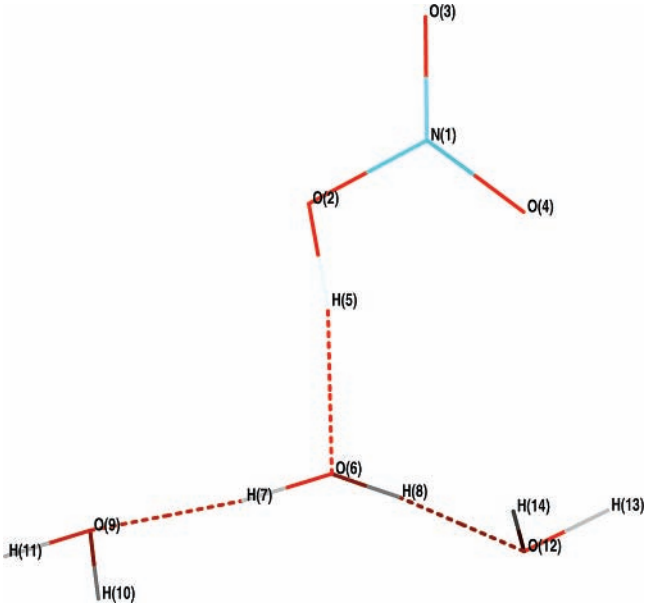

Figure 1. Core reaction system (CRS) atomic labeling.

3. Dissociation of HNO_3 at an Aqueous Layer

The four cases to be examined in this section all have the hydrogen of HNO_3 H-bonded to a water molecule (cf. Figure 1) but differ by the degree of solvation of the oxygens of the nitrate group, from HNO_3 adsorbed on top of the surface with just two H-bonds, to the acid buried in the top water layer.

In all cases, we find that the 0 K TS is product-like in structure (see Figures 2−5) and slightly higher in HF energy than the PC by 0.1−0.4 kcal/mol, and the activation energy decreases from 5.8 kcal/mol (least solvated case) to 2.3 kcal/mol (most solvated case). We have examined the RC and PC of each case to highlight variations in the H-bonding pattern along the reaction path; a qualitative description of the evolution of the H-bonding pattern around the $H_2O\cdots HNO_3$ sub-CRS is given in each subsection below. Structural as well as energetic details are available as Supporting Information.

3.1. HNO_3 Atop the Surface: $HNO_3\cdot(H_2O)_3\cdot W_{33} \rightarrow NO_3^-\cdot H_3O^+\cdot(H_2O)_2\cdot W_{33}$ (I). In this first case (cf. Figure 2), the NO_3 moiety of HNO_3 is the least solvated, and this MRS is included mainly for reference because, as discussed below, minimal solvation is expected to preclude a favorable acid dissociation. This case mimics HNO_3 adsorbed on top of the aqueous surface, with an RC in which the acidic proton is H-bonded to a (quantum) surface water, itself H-bonded to two (quantum) waters (so that these three waters and the HNO_3 comprise the CRS). The HNO_3 oxygen *cis* to the proton is H-bonded to another (classical) surface water. In HNO_3, neither the proton-bearing oxygen nor the other oxygen in the NO_2 moiety are solvated in the RC.

In the evolution from RC to PC, there are two new, weak H-bonds of 2.3 Å that form, one to O(2) (cf. Figure 1, used as reference for atomic labels also in the following sections) and one between two classical waters. The two H-bonds to the H_3O^+ by O(9) and O(12) are reduced from 1.8 to 1.6 Å, whereas the H-bond to O(6) of the ensuing hydronium is replaced by an

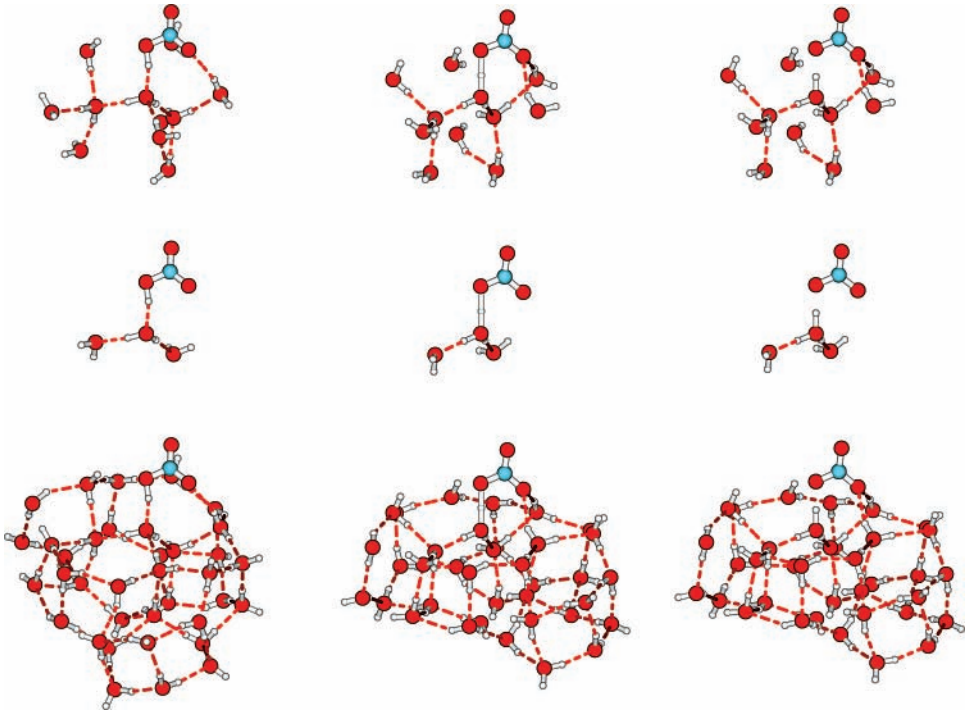

Figure 2. **I**, $HNO_3 \cdot (H_2O)_3 \cdot W_{33} \rightarrow NO_3^- \cdot H_3O^+ \cdot (H_2O)_2 \cdot W_{33}$. From left to right: RC, TS, and PC. Bottom row: MRS. The oxygen of the proton-accepting water in the CRS within the MRS is located in the origin of the reference frame of the MRS. The proton-bearing O of HNO_3 is positioned on the positive *x* semi-axis, lying within the page. The N is located in the plane of the page. Middle row: CRS only, shifted by 10 Å above its image within the MRS. Same orientation as the MRS applies. Top row: CRS plus solvating waters used for the MP2 estimate of electron correlation (see Table 7), shifted by 22 Å above its image within the MRS. All structures are provided as Supporting Information.

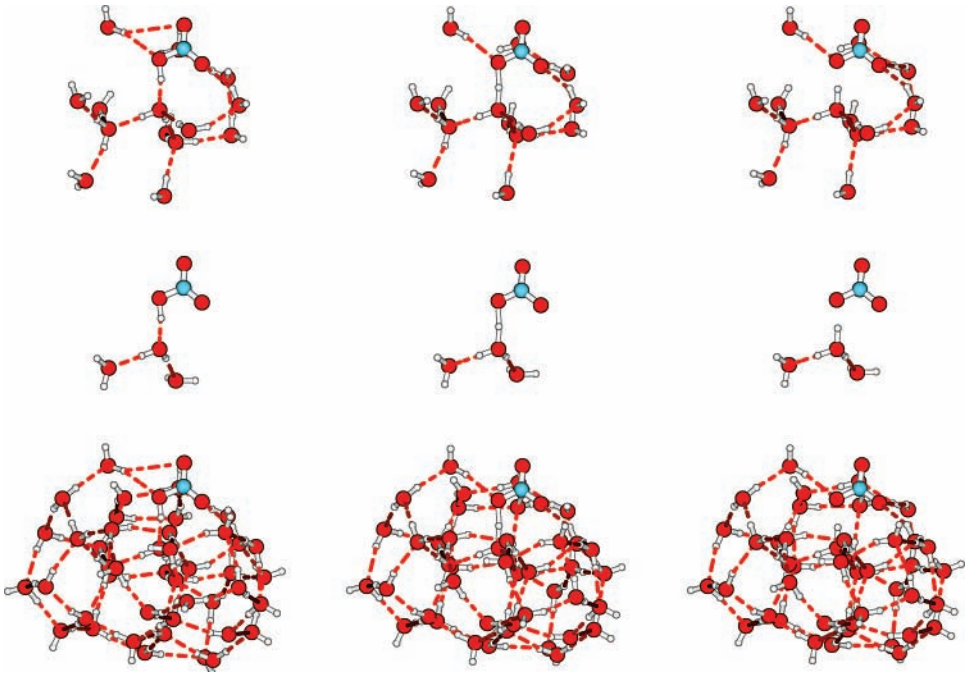

Figure 3. **II**, $HNO_3 \cdot (H_2O)_3 \cdot W_{40} \rightarrow NO_3^- \cdot H_3O^+ \cdot (H_2O)_2 \cdot W_{40}$. See Figure 2 for explanation.

H-bond to the nitrate group O(4). The latter is in addition to an already present H-bond to O(4). There are no H-bonds to O(3). These H-bond variations are consistent with CIP formation and the lack of solvation for the nitrate group oxygens.

This acid dissociation process is strongly endothermic, with an energy increase (at 0 K) from the RC to the PC of $\Delta E_{HF} \sim 5.57$ kcal/mol. To assess electronic correlation effects for this case, as discussed in general terms in section 2, we have employed a sub-MRS system comprising the CRS with an hydration complement of 11 waters (see Figure 2 and Table 7), with all waters treated quantum chemically. First, single point HF calculations on this sub-system have been performed for the reactant and product complexes at their HF geometries. These give a $\Delta E(0\ K)$ reaction energy of $+6.21$ kcal/mol. Single point MP2 calculations using the same structure give instead the 0 K reaction energy as 0.59 kcal/mol, providing a correction of -5.62 kcal/mol. Finally, to this is added the correction $+4.92$ kcal/mol derived from the intrinsic reaction energy correction in Table 6 from proton affinity considerations, to give a final electron correlation correction of -0.70 kcal/mol, to be applied

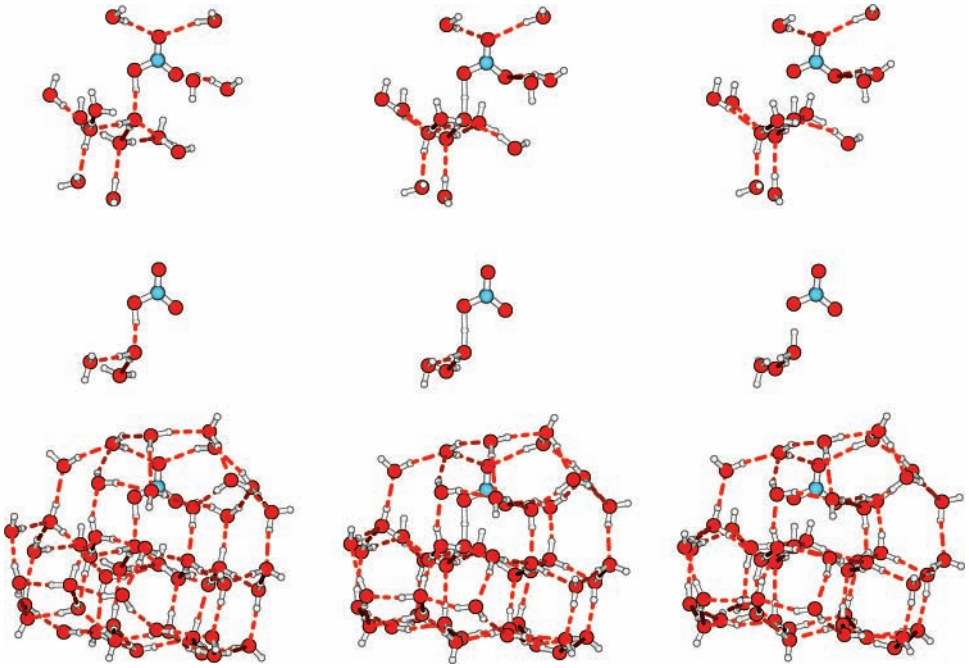

Figure 4. **III**, $HNO_3 \cdot (H_2O)_3 \cdot W_{45} \rightarrow NO_3^- \cdot H_3O^+ \cdot (H_2O)_2 \cdot W_{45}$. See Figure 2 for explanation.

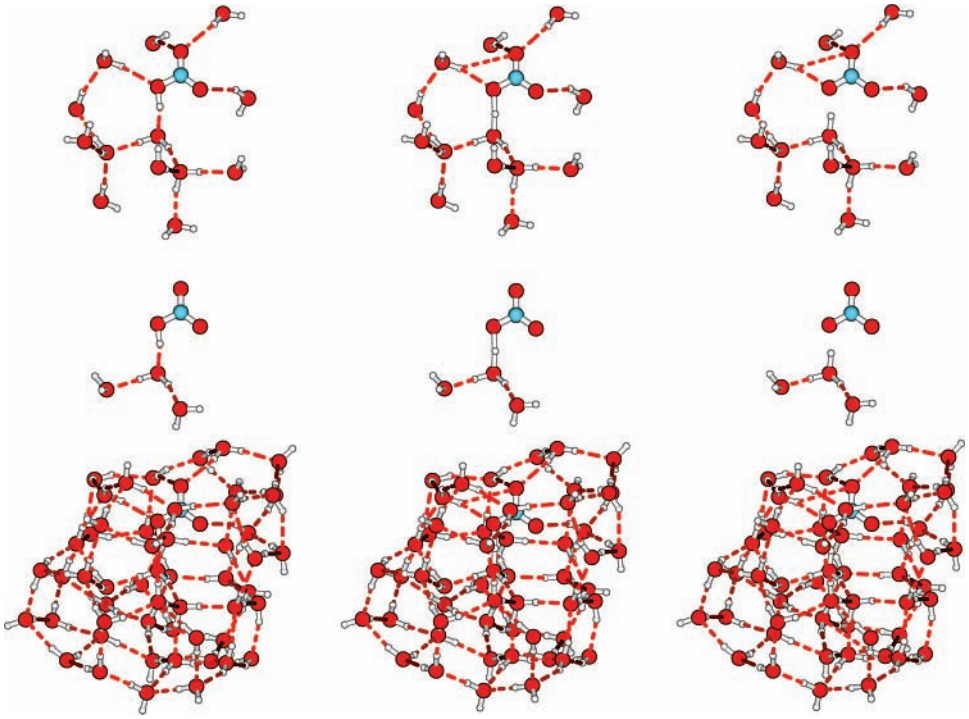

Figure 5. **IV**, $HNO_3 \cdot (H_2O)_3 \cdot W_{50} \rightarrow NO_3^- \cdot H_3O^+ \cdot (H_2O)_2 \cdot W_{50}$. See Figure 2 for explanation.

to the ΔE_{HF} of Table 8 (calculated using frequencies scaled as detailed in section 2). Thus, the final estimate of the 0 K reaction energy ΔE for the on-top case is $\Delta E = \Delta E_{HF} - 0.70$ kcal/mol $= 4.87$ kcal/mol, again indicating the strongly endothermic character of the HNO_3 acid dissociation. As is evident from Table 8, ZPE and thermal effects do not change this basic conclusion; for example, ΔH is 4.12 kcal/mol at 300 K.

To this enthalpic opposition to the acid ionization is added an unfavorable entropy change ΔS, consistent with expectations for the formation of a CIP, which increases in magnitude with temperature. For example, ΔG at 300 K is 5.57 kcal/mol (Table 8).

Before proceeding to other arrangements of HNO_3 at the surface, we pause to place the above result in some perspective. The failure of nitric acid to dissociate in these conditions can be compared with the finding[16] that the stronger acid H_2SO_4 fails to ionize in similar circumstances atop an aqueous layer. The even stronger acid HCl fails to ionize atop an aqueous surface, even with the further direct solvation, beyond that by the H_3O^+ ion, by a single water of the incipient anion;[26] HBr, the strongest acid of all those discussed here, is found, however, to ionize in such a situation.[26] Solvation of the Cl moiety of HCl by two waters can lead to acid ionization atop an aqueous surface.[26,39] In the arrangement in Figure 2, the NO_2 moiety

TABLE 8: Energetics and Thermodynamics of HNO_3 Dissociation at Model Water Layers[a]

	30 K	60 K	90 K	120 K	150 K	180 K	210 K	240 K	270 K	300 K
					I: $HNO_3{\cdot}(H_2O)_3{\cdot}W_{33} \rightarrow NO_3^-{\cdot}H_3O^+{\cdot}(H_2O)_2{\cdot}W_{33}$					
ΔG	4.63	4.68	4.75	4.84	4.93	5.05	5.17	5.29	5.42	5.57
ΔH	4.60	4.56	4.52	4.47	4.41	4.36	4.30	4.23	4.17	4.12
ΔS	−1.06	−1.98	−2.61	−3.09	−3.49	−3.83	−4.15	−4.41	−4.65	−4.85
	$\Delta E_{HF} = 5.57$		$\Delta E = 4.87$		$\Delta E + \Delta ZPE = 4.62$					
					II: $HNO_3{\cdot}(H_2O)_3{\cdot}W_{40} \rightarrow NO_3^-{\cdot}H_3O^+{\cdot}(H_2O)_2{\cdot}W_{40}$					
ΔG	1.72	1.88	2.09	2.33	2.58	2.85	3.14	3.45	3.75	4.08
ΔH	1.59	1.50	1.42	1.35	1.26	1.17	1.08	0.99	0.89	0.80
ΔS	−4.38	−6.35	−7.41	−8.19	−8.81	−9.35	−9.82	−10.23	−10.60	−10.92
	$\Delta E_{HF} = 2.88$		$\Delta E = 0.91$		$\Delta E + ZPE = 1.65$					
					III: $HNO_3{\cdot}(H_2O)_3{\cdot}W_{45} \rightarrow NO_3^-{\cdot}H_3O^+{\cdot}(H_2O)_2{\cdot}W_{45}$					
ΔG	2.91	3.04	3.20	3.39	3.60	3.82	4.07	4.33	4.60	4.89
ΔH	2.80	2.74	2.68	2.61	2.52	2.41	2.30	2.18	2.06	1.93
ΔS	−3.74	−5.04	−5.80	−6.51	−7.20	−7.84	−8.43	−8.96	−9.43	−9.86
	$\Delta E_{HF} = 2.09$		$\Delta E = 1.06$		$\Delta E + ZPE = 2.85$					
					IV: $HNO_3{\cdot}(H_2O)_3{\cdot}W_{50} \rightarrow NO_3^-{\cdot}H_3O^+{\cdot}(H_2O)_2{\cdot}W_{50}$					
ΔG	2.06	2.05	2.06	2.10	2.15	2.22	2.31	2.43	2.54	2.67
ΔH	2.08	2.04	1.98	1.91	1.83	1.74	1.64	1.55	1.44	1.33
ΔS	0.77	−0.15	−0.91	−1.55	−2.14	−2.69	−3.20	−3.66	−4.08	−4.46
	$\Delta E_{HF} = 2.06$		$\Delta E = 1.01$		$\Delta E + ZPE = 2.08$					

[a] Reaction energy ΔE, free energy ΔG, enthalpy ΔH, and zero point energy difference ΔZPE in kcal/mol. Reaction entropy ΔS in cal mol^{-1} K^{-1}. Thermal contributions calculated using frequencies scaled as described in section 2.

has only one water directly solvating a negatively charged oxygen. In the cases examined below, additional solvation of the NO_2 moiety of HNO_3 will be present, due to the embedding of the molecule in the surface region, and can be expected to assist the acid ionization.

3.2. HNO_3 Semiembedded: $HNO_3{\cdot}(H_2O)_3{\cdot}W_{40} \rightarrow NO_3^-{\cdot}H_3O^+{\cdot}(H_2O)_2{\cdot}W_{40}$ (II). In Figure 3 we show the MRS and the CRS for the dissociation of an HNO_3 which is semiembedded in the lattice with an extra water coordinated to the O(2) and double H-bonding to the nitrate O(4).

Similar to the previous case, the largest variations in H-bonding on going from RC to PC involve the two H-bonds to the hydronium cation, decreasing by about −0.2 Å to 1.5 and 1.6 Å, respectively, whereas one of the two H-bonds to the hydronium O(6) weakens and the other switches to the nitrate O(2). Formation of the nitrate anion also involves the significant strengthening of the H-bonds to O(2) and O(4) oxygens. As in the previous case, there are no H-bonds involving O(3) due to the special structural arrangement of the RC emphasizing lack of solvation for O(3).

Also in this case, the reaction at 0 K is endothermic at the HF level, with a ΔE_{HF} of 2.88 kcal/mol. The electron correlation correction of this value follows the same procedure as in section 3.1, via single point HF and MP2 calculations on the sub-MRS $HNO_3{\cdot}(H_2O)_{14}$ (cf. Figure 3 and Table 7). These give an energy difference at 0 K $E_{MP2} - E_{HF} = -5.21 - 1.68 = -6.89$ kcal/mol, which, after addition of 4.92 kcal/mol resulting from Table 6, yields a correction of −1.97 kcal/mol. The final 0 K reaction energy $\Delta E = \Delta E_{HF} - 1.97$ kcal/mol is obtained. It is this ΔE value that is displayed and employed in the results collected in Table 8.

The acid dissociation is endothermic at 0 K, $\Delta E + \Delta ZPE = 1.65$ kcal/mol, with ΔZPE contributing ∼0.7 kcal/mol to this. The reaction endothermicity is reduced as T increases, with ΔH declining to 0.8 kcal/mol at 300 K (Table 8). However, Table 8 also shows that the unfavorable reaction entropy ΔS increases in magnitude with T such that the reaction free energy at 300 K is substantial: $\Delta G = 4.08$ kcal/mol.

3.3. Further HNO_3 Embedding: $HNO_3{\cdot}(H_2O)_3{\cdot}W_{45} \rightarrow NO_3^-{\cdot}H_3O^+{\cdot}(H_2O)_2{\cdot}W_{45}$ (III). In the MRS for our next case (cf. Figure 4), HNO_3 is further embedded and the nitrate group is H-bonded via two H-bonds to each of the Os of the NO_2 moiety, albeit without H-bonding at O(2). The acidic H of HNO_3 is H-bonded to O(6) in the RC, itself H-bonded to two more waters.

Along the reaction path from RC to PC, as in the previous cases, H-bonding to the ensuing hydronium ion strengthens for its hydrogens and decreases for its oxygen. There are no H-bonds to O(2) except the one from H_3O^+. The existing H-bond to the nitrate O(3) registers minimal change, and the other nitrate oxygen, O(4), without H-bonds in the RC, forms a new H-bond of 2.16 Å.

As in the previous two cases, the acid dissociation at 0 K is again endothermic at the HF level: the reaction energy $\Delta E_{HF} = 2.09$ kcal/mol. Electron correlation corrections to the HF energy are assessed as in sections 3.1 and 3.2 via single-point energy calculations on the $HNO_3{\cdot}(H_2O)_{14}$ sub-MRS in Figure 4. Use of the values in Table 7 yields a correction of −1.03 kcal/mol to be applied to the ΔE_{HF} in Table 8, so that the 0 K electronic reaction energy is $\Delta E = 1.06$ kcal/mol; addition of the ZPE correction $\Delta ZPE = 1.79$ kcal/mol to this then gives the 0 K reaction energy as 2.85 kcal/mol (Table 8).

The thermodynamic reaction quantities (Table 8, see section 2 for details on frequency scaling) follow the same trends as for the first two cases already discussed. The reaction remains endothermic throughout the temperature range up to 300 K, though the reaction enthalpy ΔH diminishes throughout the range; ΔH(300 K) is lower than ΔH(0 K) by about 0.9 kcal/mol, but this reduction is more than compensated for by the increasingly unfavorable reaction entropy ΔS as T increases, with ΔG rising to a value of 4.89 kcal/mol at 300 K.

3.4. Maximally Solvated HNO_3: $HNO_3{\cdot}(H_2O)_3{\cdot}W_{50} \rightarrow NO_3^-{\cdot}H_3O^+{\cdot}(H_2O)_2{\cdot}W_{50}$ (IV). Our final case (cf. Figure 5) examines the effects of H-bonding to all the Os of the nitrate group, with HNO_3 further embedded in the water lattice. Of all the cases considered, this MRS has the maximum solvation of the nitrate group and, consequently, has the maximum number of water molecules.

In the acid dissociation transition from the RC to the PC (Figure 5), both H-bonds to the hydronium hydrogens decrease sharply by −0.2 Å to 1.6 and 1.5 Å, respectively, whereas that to O(6) increases by a comparable amount to 2.1 Å. A second

H-bond to the nitrate O(2), in addition to that from hydronium, also strengthens. Due to the increased surface solvation of the nitrate group in this case, O(3) in the PC bears two H-bonds in the 2.1−2.2 Å range, and the single H-bond to O(4) decreases by 0.1 Å to 2.1 Å.

As with the preceding three cases, the acid dissociation is endothermic at the HF level at 0 K: $\Delta E_{HF} = 2.06$ kcal/mol (Table 8). The procedure for the inclusion of electron correlation effects used in the preceding three cases yields a net correction of −1.05 kcal/mol to the 0 K HF reaction energy, giving the corrected electronic reaction energy $\Delta E = 1.01$ kcal/mol; the addition of the ZPE correction ΔZPE = 1.07 kcal/mol to this gives the 0 K reaction energy as 2.08 kcal/mol (Table 8).

The behavior of the reaction thermodynamic quantities from 0 to 300 K (Table 8) is, with the exception of the 30 K results (ignored in the following discussion), similar to that of the preceding cases. The reaction endothermicity monotonically decreases with increasing T to drop to the modest value of $\Delta H = 1.33$ kcal/mol at 300 K. Again, the reaction entropy is unfavorable and its increasing magnitude gives the maximum unfavorable free energy at 300 K as $\Delta G = 2.67$ kcal/mol. Because this corresponds to an equilibrium constant of approximately 10^{-2} at 300 K for the ion pair formation, nitric acid will remain almost completely molecular. Similar considerations apply in the temperature range 205−265 K relevant for the upper troposphere.[28]

3.5. Overview. HNO_3 acid ionization is thermodynamically disfavored in each of the four cases examined: the reaction free energy ΔG is positive and monotonically increasing in the entire temperature range 0−300 K considered (cf. Table 8). The patterns of the cases **I**, least solvated, and **IV**, most solvated, are consistent: $\Delta G_{\mathbf{I}}$ is always higher than $\Delta G_{\mathbf{IV}}$, the difference rising to ∼3 kcal/mol at 300 K. The two intermediate cases, **II** and **III**, are somewhat anomalous, because **II** lacks solvation on one of the two NO_2 oxygens, whereas **III** lacks solvation on the H^+-bearing oxygen. $\Delta G_{\mathbf{II}}$ is lower than $\Delta G_{\mathbf{IV}}$ up to a bit below 90 K, but higher in the remainder of the temperature range. $\Delta G_{\mathbf{III}}$ is higher than $\Delta G_{\mathbf{IV}}$ at all temperatures. This particular comparison suggests that H-bonding to the H^+-bearing oxygen of HNO_3 plays a key role in promoting dissociation. Overall, the acid dissociation becomes less disfavored with increasing solvation of the NO_3 moiety of the nitric acid molecule.

The reaction is endothermic in all four cases over the entire temperature range: the reaction enthalpy ΔH decreases monotonically with T from its 0 K value $\Delta E + \Delta$ZPE. For the least solvated case **I**, this is a decrease by ∼0.5 kcal/mol to a 300 K ΔH value ∼4.1 kcal/mol, whereas for the most solvated case **IV**, there is a decrease of ∼0.8 kcal/mol to a 300 K value ∼1.3 kcal/mol. These thermal contributions to ΔH are naturally dominated by vibrational frequencies below 1000 cm^{-1}, with the most important role played by intermolecular vibrations, with the contribution of the EFP waters typically playing the most significant role (see Supporting Information). In contrast, the zero point energy contributions ΔZPE to the 0 K value $\Delta E + \Delta$ZPE, which in the least solvated case **I**, is only 0.25 kcal/mol and for the most solvated case, **IV**, is ∼+1.1 kcal/mol, typically having significant contributions both below and above 1000 cm^{-1}, with the EFP intermolecular vibrations contribution being somewhat more important than that of the CRS intra- and intermolecular vibrations (an exception is case **I**, where these two nearly cancel each other).

With one exception (case **IV**, 30 K in Table 8), the reaction entropy ΔS is always negative and monotonically decreasing with increasing T, as expected, due to the formation of a contact ion pair from a neutral pair. This increasingly unfavorable reaction entropy trend is also reflected by the decreasing lengths of the H-bonds to the nitrate group going from reactants to products (see Supporting Information for structures of the clusters displayed in the top rows of Figures 2−5). The trend is also significant for the reaction free energy; for example, the thermal enthalpic and entropic contributions for case **IV** are essentially identical at 300 K, so that ΔG is only slightly larger than the 0 K reaction energy $\Delta E + \Delta$ZPE. In all four cases and at all temperatures, the entropy change is dominated by contributions from intermolecular vibrations of less than 1000 cm^{-1} (and concentrated below 400 cm^{-1}), with CRS intramolecular vibrations playing a negligible role; the dominant intermolecular modes are those of the EFP waters (see Supporting Information). The uniform variation of all the vibrational frequencies used for the calculation of Table 8 by ±5% yields values of ΔG, ΔH, and ΔZPE differing by less than ±0.1 kcal/mol and ΔS values differing by less than ±0.2 cal mol^{-1} K^{-1} at all temperatures and for all four cases, thus strengthening our conclusions.

4. HNO_3 Band Assignments in $HNO_3 \cdot (H_2O)_3 \cdot W_{33,50}$

As noted in the Introduction, several experiments,[17−19,21,22] including some employing surface-sensitive spectroscopic techniques,[18−19, 21−22] have concluded that molecular HNO_3 is dominant at the surface of concentrated nitric acid solutions (for which molecular nitric acid is also dominant in the bulk[23,24]). Surface sensitive spectroscopic results are also available for lower concentration nitric acid solutions, more closely approaching the conditions of the present calculations, for which HNO_3 is found to remain molecular, and are now discussed.

The pioneering Schultz group surface spectroscopy experiments on aqueous HNO_3 solutions in the high-frequency OH stretch region[18,19,21] included (in addition to highly concentrated solutions where molecular HNO_3 was inferred to be present in the surface layer) examination of quite dilute solutions—HNO_3 mole fraction 0.05 and below[18]—which would be most appropriate for comparison with the present study. Although it was concluded that, at the highest concentration in this range, the surface layer was modified by a sufficiently close approach of HNO_3 molecules or ionic complexes, a clear picture of the character of surface HNO_3 did not emerge.[40]

Very recently, Kido Soule et al.,[22] via vibrational sum-frequency spectroscopy (VSFS) of HNO_3/H_2O solutions, have argued in favor of the presence of molecular nitric acid at the vapor/solution interface at concentrations down to 10 mol %, where the ratio HNO_3:NO_3^- is estimated to be 1:3.[22] They have assigned (i) one spectral feature at 1690 cm^{-1} to the NO_2 asymmetric stretch ν_{NO_2} of HNO_3 in a monohydrate complex in the topmost surface layer, and (ii) a second spectral feature at 1662 cm^{-1} to a more strongly H-bonded $HNO_3 \cdot (H_2O)_n$ complex, presumably deeper in the interfacial region.

Our model systems **I** (section 3.1) and **IV** (section 3.4) are representative of the two kinds of HNO_3 interfacial solvation proposed in ref 22. We have analyzed the vibrational signatures of HNO_3 and NO_3^- in the RC and the (disfavored) PC, respectively, of cases **I** (HNO_3 on top) and **IV** (HNO_3 deeper in the interfacial layer). For both cases, we have identified the ν_{NO_2} mode for both HNO_3 and NO_3^- and scaled the HF frequencies by the ν_{NO_2} mode-specific scaling factor 0.8848 for HNO_3, according to Table 2. For HNO_3 in **I**, we find ν_{NO_2} 1704 cm^{-1}, whereas for HNO_3 in **IV** we find ν_{NO_2} 1675 cm^{-1}, compared to 1690 and 1662 cm^{-1}, respectively, assigned in ref

22. Further, the 1704 and 1675 cm^{-1} peaks are derived for HNO_3 in two different environments, but essentially in the same orientation with respect to the aqueous layer, thus supporting the conclusion in ref 22 that transition strengths (modulated by solvation) and concentration at the surface, rather than HNO_3 orientation, are responsible for the two different peaks. For the NO_3^- ν_{NO_2} mode in **I** and **IV**, we have calculated 1327 and 1495 cm^{-1}, respectively, markedly red-shifted with respect to, and thus clearly distinguishable from, the HNO_3 bands—these values indirectly strengthen the assignments by Kido Soule et al.[22]

In summary, these frequency calculations support our free energy-based conclusions concerning molecular HNO_3 and are consistent with the conclusions of ref 22. A detailed analysis of the vibrational signatures of the HNO_3, NO_3^-, H_2O, and H_3O^+ in the MRS **I**−**IV** examined here will be presented elsewhere.[41]

5. Concluding Remarks

The calculated reaction free energies for the dissociation of nitric acid $HNO_3 + H_2O \rightarrow NO_3^- + H_3O^+$ on/at model aqueous surfaces for four cases with varying degrees of solvation indicate that HNO_3 remains molecular, rather than acid dissociated, over the entire temperature range 0−300 K. (After the present paper was submitted, we received a preprint[42] in which Car−Parrinnelo molecular dynamics simulations indicate that at room-temperature HNO_3 remains molecular at an aqueous surface.) The 300 K free energies ΔG for the acid dissociation range from 5.57 kcal/mol for HNO_3 atop the surface, with the least solvation of the nitrate ion, to 2.67 kcal/mol for the surface-embedded, most solvated situation for this ion. In all four cases, the proton-transfer reaction is endothermic ($\Delta H > 0$) and is entropically disfavored ($\Delta S < 0$) at 300 K, with the latter aspect consistent with increased strength of H-bonding in the ion pair products compared to the molecular reactants. All these thermodynamic features also apply at the lower temperatures 206−264 K relevant for nitric acid uptake in the upper troposphere[5−14,28] and in other atmospheric/environmental venues, mentioned in the Introduction, where the nitric acid dissociation issue is important.[3,4,43−45] The unfavorable reaction free energy decreases as the temperature is lowered, a behavior due to the diminution of the magnitude of the unfavorable reaction entropy ΔS (for related examples, see refs 16 and 69).

These results are consistent with similar earlier calculations[16,27] for sulfuric acid H_2SO_4, which is a stronger acid than is HNO_3 in aqueous solution,[15] where the first acid dissocation of H_2SO_4 at an aqueous interface was found to be unfavorable in certain higher temperature ranges even with significant embedding of the acid. They are also consistent with the very recent surface-sensitive sum frequency generation spectroscopic results from the Richmond group,[22] which indicated the presence of molecular nitric acid at the surfaces of moderately dilute aqueous nitric acid solutions which, though having a bulk concentration higher than the present calculations, are nonetheless lower in concentration than those where molecular nitric acid is known to dominate in the bulk solution.[23,24] Further, nitric acid asymmetric NO_2 stretch frequency calculations for the two cases of minimal and maximal NO_3 moiety solvation (cases **I** and **IV**, respectively) are consistent with the interpretation given in ref 22 for differing molecular nitric acid solvation scenarios. A detailed discussion of the vibrational spectroscopic features of all the species involved in the nitric acid dissociation for the four cases discussed within will be presented elsewhere.[41] This should prove useful for both the further interpretation of existing surface-sensitive spectroscopic experiments[18,19,21,22] and theoretical construction and analysis [46−50]of these spectra.

Further, several recent classical molecular dynamics simulations have been concerned with the issue of the spatial distribution of the nitrate ion NO_3^- at an aqueous surface region of $NaNO_3$ solutions.[51−53] The consensus reached in the most recent of these studies[53] is that NO_3^- is located mainly in the bulk of the solution, with very little NO_3^- in the surface region. Although this[53] and previous studies[51,52] obviously do not address the nitric acid dissociation problem, the avoidance by NO_3^- of the aqueous interfacial region implies a less effective solvation there than in the bulk, an aspect that would play a contributing role to the dominance of molecular nitric acid at the surface found in the present work.

The present results suggest that the uptake of nitric acid by water ice aerosols in the upper troposphere occurs by a molecular, rather than an ionic, mechanism, at least initially. One could nonetheless imagine that the originally suggested acid ionization mechanism[10] could become involved either by diffusion of molecular HNO_3 deeper into the aerosol[54] where it could dissociate or by a "burying" of the molecular HNO_3 by accreting water molecules at a dynamic ice surface,[55,56] in each case benefiting from increased solvation of the HNO_3, and especially of its NO_3 moiety. We also note that, because the present results are limited to a single HNO_3 moiety, they are not directly applicable to aerosols in the upper troposphere under conditions where significant HNO_3 uptake has occurred; [10,12−14] this issue is under study via a reactive Monte Carlo methodology.[57] Knowledge of whether or not molecular nitric acid persists under these conditions[58] is clearly key for future theoretical modeling of heterogeneous reactions on such aerosol surfaces important for ozone depletion, e.g., the reaction between HCl and $ClONO_2$.[2,25,59,60]

We also need to remark that several effects not included in the present calculations merit further investigation. The first is that the zero point energies and thermodynamic contributions to the reaction free energies/enthalpies/entropies have been calculated in the harmonic approximation for the vibrations calculated at 0 K geometries. At higher temperatures, particularly for the lower frequency vibrations, anharmonicities will become important and the hydration structures will change. It is difficult to assess the net importance of these effects except to note that, in a general way, one expects the solvation effects to diminish in magnitude with increasing temperature, which would imply that the HNO_3 acid ionization would become even less favorable; in addition, the unfavorable entropy change (cf. Table 8) is likely to become more pronounced. The second, countervailing effect is that computational considerations have restricted the size of the systems we have been able to model. Addition of further waters would provide more solvation, favoring to some degree the nitric acid dissociation. These are likely not to be large given the size of the current systems (although we have not been able to reliably estimate them quantitatively[61]); the non-negligible values of the reaction free energies for the various cases examined (cf. Table 8) indicate that further solvation effects would have to be fairly substantial to have an impact on the present conclusions.

Acknowledgment. This work was supported in part by NSF grant CHE-0417570. J.T.H. also acknowledges support via an ANR grant (NT05-4-43154) and ECOS grant A01U03.

Supporting Information Available: (1) Structural comparisons of the optimized complexes $HNO_3 \cdot (H_2O)_2$ vs $HNO_3 \cdot H_2O \cdot W$ and $NO_3^- \cdot H_2O$ vs $NO_3^- \cdot W$. (2) Structures and energy (at 0 K) of the RC, TS, and PC of the CRS/MRS as displayed in Figures 2−5. (3) Changes in H-bonding patterns from RC to

PC. (4) Vibrational frequency contributions to ΔS, ΔH, and ΔZPE in the 0-400, 400-800, and >800 cm^{-1} intervals. (5) Vibrational mode contributions to ΔH, ΔS, and ΔG. This material is available free of charge via the Internet at http://pubs.acs.org.

References and Notes

(1) Solomon, S. *Rev. Geophysics* **1999**, *37*, 275.

(2) Bianco, R.; Hynes, J. T. *J. Phys. Chem. A* **1999**, *103*, 3797.

(3) (a) Rivera-Figueroa, A. M.; Sumner, A. L.; Finlayson-Pitts, B. J. *Environ. Sci. Technol.* **2003**, *37*, 548. (b) Mochida, M.; Finlayson-Pitts, B. J. *J. Phys. Chem. A* **2000**, *104*, 9705. (c) Saliba, N. A.; Yang, H.; Finlayson-Pitts, B. J. *J. Phys. Chem. A* **2001**, *105*, 10339.

(4) (a) Guimbaud, C.; Arens, F.; Gutzwiller, L.; Gäggeler, H. W.; Ammann, M. *Atmos. Chem. Phys. Discuss.* **2002**, *2*, 739. (b) Davies, J. A.; Cox, R. A. *J. Phys. Chem. A* **1998**, *102*, 7631. (c) Beichert, P.; Finlayson-Pitts, B. J. *J. Phys. Chem. A* **1996**, *100*, 15218. (d) Ghosal, S.; Hemminger, J. C. *J. Phys. Chem. B* **2004**, *108*, 14102.

(5) Meilinger, S. K.; Kärcher, B.; Peter, Th. *Atmos. Chem. Phys. Discuss.* **2004**, *4*, 4455.

(6) Lawrence, M. G.; Crutzen, P. J. *Tellus* **1998**, *50B*, 263.

(7) Solomon, S.; Borrmann, S.; Garcia, R. R.; Portmann, R.; Thomason, L.; Poole, L. R.; Winker, D.; McCormick, M. P. *J. Geophys. Res.* **1997**, *102*, 21411.

(8) Borrmann, S.; Solomon, S.; Dye, J. E.; Luo, B. P. *Geophys. Res. Lett.* **1996**, *23*, 2133.

(9) Meier, A.; Hendricks, J. *J. Geophys. Res.* **2002**, *107* (D23), Art. no.4696.

(10) Abbatt, J. P. D. *Geophys. Res. Lett.* **1997**, *24*, 1479.

(11) It is an important point that nitric acid trihydrate (NAT), which is often implicated in the stratosphere, is not thermodynamically stable under upper troposphere conditions, so that the formation of such a stable hydrate cannot be invoked as an explanation for the ready uptake.

(12) Zondlo, M. A.; Barone, S. B.; Tolbert, M. A. *Geophys. Res. Lett.* **1997**, *24*, 1391.

(13) Zondlo, M. A.; Hudson, P. K.; Prenni, A. P.; Tolbert, M. A. *Annu. Rev. Phys. Chem.* **2000**, *51*, 473.

(14) Hudson, P. K.; Shilling, J. E.; Tolbert, M. A.; Toon, O. B. *J. Phys. Chem. A* **2002**, *106*, 9874.

(15) Oxtoby, D. W.; Nachtrieb, N. H. *Principles of Modern Chemistry*, 2nd ed.; Saunders: Philadelphia, 1990.

(16) Bianco, R.; Wang, S.; Hynes, J. T. *J. Phys. Chem. B* **2005**, *109*, 21313.

(17) (a) Donaldson, D. J.; Anderson, D. *Geophys. Res. Lett.* **1999**, *26*, 3625. (b) Clifford, D.; Bartels-Rausch, T.; Donaldson, D. J. *Phys. Chem. Chem. Phys.* **2007**, *9*, 1362.

(18) Schnitzer, C.; Baldelli, S.; Shultz, M. J. *Chem. Phys. Lett.* **1999**, *313*, 416.

(19) Shultz, M. J.; Schnitzer, C.; Simonelli, D.; Baldelli, S. *Int. Rev. Phys. Chem.* **2000**, *18*, 123.

(20) Yang, H. S.; Finlayson-Pitts, B. J. *J. Phys. Chem. A* **2001**, *105*, 1890.

(21) Shultz, M. J.; Baldelli, S.; Schnitzer, C.; Simonelli, D. *J. Phys. Chem. B* **2002**, *106*, 5313.

(22) Soule, M. C. K.; Blower, P. G.; Richmond, G. L. *J. Phys. Chem. A* **2007**, *111*, 3349.

(23) Young, T. F.; Maranville, L. F.; Smith, H. M. In *The Structure of Electrolyte Solutions*; Hamer, W. J.; Ed.; Wiley and Sons: New York, 1959; Chapter 4.

(24) Minogue, N.; Riordan, E.; Sodeau, J. R. *J. Phys. Chem. A* **2003**, *107*, 4436.

(25) Bianco, R.; Hynes, J. T. *Acc. Chem. Res.* **2006**, *39*, 159.

(26) Al-Halabi, A.; Bianco, R.; Hynes, J. T. *J. Phys. Chem. A* **2002**, *106*, 7639. For HCl, see also ref 55.

(27) Bianco, R.; Hynes, J. T. *Theor. Chem. Acc.* **2004**, *111*, 182.

(28) Evans, K. D.; Melfi, S. H.; Ferrare, R. A.; Whiteman, D. N. *Appl. Opt.* **1997**, *36*, 2594.

(29) (a) Day, P. N.; Jensen, J. H.; Gordon, M. S.; Webb, S. P.; Stevens, W. J.; Krauss, M.; Garmer, D.; Basch, H.; Cohen, D. *J. Chem. Phys.* **1996**, *105*, 1968. (b) Chen, W.; Gordon, M. S. *J. Chem. Phys.* **1996**, *105*, 11081.

(30) Stevens, W. J.; Basch, H.; Krauss, M. *J. Chem. Phys.* **1984**, *81*, 6026.

(31) Pietro, W. J.; Francl, M. M.; Hehre, W. J.; DeFrees, D. J.; Pople, J. A.; Binkley, J. S. *J. Am. Chem. Soc.* **1982**, *104*, 5039.

(32) Clark, T.; Chandrasekhar, J.; Spitznagel, G. W.; Schleyer, P. v. R. *J. Comput. Chem.* **1983**, *4*, 294.

(33) Schmidt, M. W.; Baldridge, K. K.; Boatz, J. A.; Elbert, S. T.; Gordon, M. S.; Jensen, J. H.; Koseki, S.; Matsunaga, N.; Nguyen, K. A.; Su, S. J.; Windus, T. L.; Dupuis, M.; Montgomery, J. A. *J. Comput. Chem.* **1993**, *14*, 1347.

(34) Elola, M. D.; Marceca, E. J.; Laria, D.; Estrin, D. A. *Chem. Phys. Lett.* **2000**, *326*, 509.

(35) Ishida, K.; Morokuma, K.; Komornicki, A. *J. Chem. Phys.* **1977**, *66*, 2153 and references therein.

(36) Schaftenaar, G.; Noordik, J. H. *Molden: a pre- and post-processing program for molecular and electronic structures J. Comput. Aided Mol. Design* **2000,** *14*, 123. Molden is available free of charge for academic use at http://www.cmbi.ru.nl/molden/molden.html.

(37) Xantheas, S. S.; Dunning, T. H., Jr. *J. Chem. Phys.* **1993**, *99*, 8774.

(38) Petersson, G. A.; Bennett, A.; Tensfeldt, T. G.; Al-Laham, M. A.; Shirley, W. A. *J. Chem. Phys.* **1988**, *89*, 2193. Montgomery, J. A., Jr.; Ochterski, J. W.; Petersson, G. A. *J. Chem. Phys.* **1994**, *101*, 5900. Ochterski, J. W.; Petersson, G. A.; Montgomery, J. A., Jr. *J. Chem. Phys.* **1996**, *104*, 2598. Montgomery, J. A., Jr.; Frisch, M. J.; Ochterski, J. W.; Petersson, G. A. *J. Chem. Phys.* **1999**, *110*, 2822. Montgomery, J. A., Jr.; Frisch, M. J.; Ochterski, J. W.; Petersson, G. A. *J. Chem. Phys.* **2000**, *112*, 6532.

(39) (a) Svanberg, M.; Pettersson, J. B. C.; Bolton, K. *J. Phys. Chem. A* **2000**, *104*, 5787. (b) Devlin, J. P.; Uras, N.; Sadlej, J.; Buch, V. *Nature* **2002**, *417*, 269. (c) Bolton, K. *Int. J. Quantum Chem.* **2004**, *96*, 607. (d) Mantz, Y. A.; Geiger, F. M.; Molina, L. T.; Molina, M. J.; Trout, B. L. *Chem. Phys. Lett.* **2001**, *348*, 285. (e) for ionization of HCl at, rather than atop, an ice surface, see ref 55.

(40) It is interesting to note that examination of the NO stretch region was advocated in ref 18 as a potential useful source of information on the HNO_3 acid dissociation issue.

(41) Bianco, R.; Wang, S.; Hynes, J. T. To be submitted.

(42) Shamay, E. S.; Buch, V.; Parrinello, M.; Richmond, G. L. At the Water's Edge: Nitric Acid as a Weak Acid, preprint, 2007.

(43) See also Ramazan, K. A.; Wingen, L. M.; Miller, Y.; Chaban, G. M.; Gerber, R. B.; Xantheas, S. S.; Finlayson-Pitts, B. J. *J. Phys. Chem. A* **2006**, *110*, 6886. Goodman, A. L.; Bernard, E. T.; Grassian, V. H. *J. Phys. Chem. A* **2001**, *105*, 6443.

(44) We should note that nitric acid dissociates in central locations in small protonated water clusters (see: D'Auria, R.; Turco, R. P.; Houk, K. N. *J. Phys. Chem. A* **2004**, *108*, 3756. Gilligan, J. J.; Castleman, A. W., Jr. *J. Phys. Chem. A* **2001**, *105*, 5601). In addition to dissociation assistance by a hydronium ion already present, such small cluster systems, including those without an excess proton (Scott, J. R.; Wright, J. B. *J. Phys. Chem. A* **2004**, *108*, 10578), can often show quite different behavior for acid dissociation than do surface system models such as the present ones.[25]

(45) In ref 2 for the reaction of $ClONO_2$ + HCl and in ref 62 for the hydrolysis of $ClONO_2$, acid-dissociated HNO_3 was found in small water cluster models of an ice surface. This may be related to a better solvation (than by a water molecule) of the nitrate ion via a soft $Cl^{\delta+}$/soft NO_3^- ionic interaction.

(46) Morita, A.; Hynes, J. T. *Chem. Phys.* **2000**, *258*, 371; *J. Phys. Chem. B* **2002**, *106*, 673.

(47) Raymond, E. A.; Tarbuck, T. L.; Brown, M. G.; Richmond, G. L. *J. Phys. Chem. B* **2003**, *107*, 546.

(48) Perry, A.; Ahlborn, H.; Space, B.; Moore, P. B. *J. Chem. Phys.* **2003**, *118*, 8411.

(49) Brown, E. C.; Mucha, M.; Jungwirth, P.; Tobias, D. J. *J. Phys. Chem. B* **2005**, *109*, 7934.

(50) Ishiyama, T.; Morita, A. *Chem. Phys. Lett.* **2006**, *431*, 78; *J. Phys. Chem. C* **2007**, *111*, 721; *J. Phys. Chem. C* **2007**, *111*, 738.

(51) Salvador, P.; Curtis, J. E.; Tobias, D. J.; Jungwirth, P. *Phys. Chem. Chem. Phys.* **2003**, *5*, 3752.

(52) Dang, L. X.; Chang, T. M.; Roeselova, M.; Garrett, B. C.; Tobias, D. J. *J. Chem. Phys.* **2006**, *124*, Art. No. 066101.

(53) Thomas, J. L.; Roeselova, M.; Dang, L. X.; Tobias, D. J. *J. Phys. Chem. A* **2007**, *111*, 3091.

(54) Toubin, C.; Picaud, S.; Hoang, P. N. M.; Girardet, C.; Lynden-Bell, R. M.; Hynes, J. T. *J. Chem. Phys.* **2003**, *118*, 9814.

(55) Gertner, B. J.; Hynes, J. T. *Science* **1996**, *271*, 1563; *Faraday. Discuss.* 1998, *110*, 301.

(56) Haynes, D. R.; Tro, N. J.; George, S. M. *J. Phys. Chem.* **1992**, *96*, 8502.

(57) Bianco, R.; Wang, S.; Hynes, J. T. Work in progress.

(58) Persistence of molecular nitric acid under such conditions is suggested by assorted laboratory experiments for concentratred nitric acid solutions surfaces.[17−19,22]

(59) McNamara, J. P.; Hillier, I. H. *J. Phys. Chem. A* **2001**, *105*, 7011.

(60) Bianco, R.; Hynes, J. T. *J. Phys. Chem. A* **2003**, *107*, 5253.

(61) An analysis (not presented here) of the entropy effects in Table 8, especially for cases **II** and **III**, which, as we have noted in section 3.5, exhibit somewhat anomalous aspects, suggests that there are certain finite

size system effects, but their precise identification in terms of molecular motions has not been achieved.

(62) Bianco, R.; Hynes, J. T. *J. Phys. Chem. A* **1998**, *102*, 309.
(63) Cox, A. P.; Riveros, J. M. *J. Chem. Phys.* **1965**, *42*, 3106.
(64) Lee, T. J. *J. Phys. Chem.* **1995**, *99*, 1943.
(65) Shimanouchi, T. *Tables of Molecular Vibrational Frequencies Consolidated*; National Bureau of Standards: Washington, DC, 1997; Vol. I, pp 1−160. 1 cm^{-1} uncertainty.
(66) Ahlijah, G. E. B. Y.; Mooney, E. F. *Spectrochim. Acta A* **1969**, *25*, 619.
(67) Huang, X. C.; Carter, S.; Bowman, J. M. *J. Phys. Chem. B* **2002**, *106*, 8182.
(68) Dixon, D. A.; Feller, D.; Zhan, C. G.; Francisco, J. S. *Int. J. Mass Spectrom.* **2003**, *227*, 421.
(69) Ayotte, P.; Hebert, M.; Marchand, P. *J. Chem. Phys.* **2005**, *123*, 184501.